

Electromagnetic propagation in a relativistic electron gas at finite temperatures

D. M. Reis¹, E. Reyes-Gómez², L. E. Oliveira³, and C. A. A. de Carvalho^{4,5}

¹*Centro Brasileiro de Pesquisas Físicas - CBPF,*

Rua Dr. Xavier Sigaud 150, Rio de Janeiro - RJ, 22290-180, Brazil

²*Instituto de Física, Universidad de Antioquia - UdeA, Calle 70 No. 52-21, Medellín, Colombia*

³*Instituto de Física, Universidade Estadual de Campinas - Unicamp, Campinas - SP, 13083-859, Brazil*

⁴*Diretoria Geral de Desenvolvimento Nuclear e Tecnológico da Marinha - DGDNTM,*

Rua da Ponte s/n, Ed. 23 do AMRJ, Rio de Janeiro - RJ, 20091-000, Brazil

⁵*Instituto de Física, Universidade Federal do Rio de Janeiro - UFRJ,*

Caixa Postal 68528, Rio de Janeiro - RJ, 21945-972, Brazil

(Dated: December 14, 2024)

We describe electromagnetic propagation in a relativistic electron gas at finite temperatures and carrier densities. Using quantum electrodynamics at finite temperatures, we obtain electric and magnetic responses and general constitutive relations. Rewriting the propagator for the electromagnetic field in terms of the electric and magnetic responses, we identify the modes that propagate in the gas. As expected, we obtain the usual collective excitations, i.e., a longitudinal electric and two transverse magnetic plasmonic modes. In addition, we find a purely photonic mode that satisfies the wave equation in vacuum, for which the electron gas is transparent. We present dispersion relations for the plasmon modes at zero and finite temperatures and identify the intervals of frequency and wavelength where both electric and magnetic responses are simultaneously negative, a behavior previously thought not to occur in natural systems.

PACS numbers: 71.10.Ca; 71.45.Gm; 78.20.Ci.

I. INTRODUCTION

The knowledge of the properties of a relativistic electron gas (REG) at finite temperatures and densities is a useful tool for understanding the physics of several systems. Investigations on the response of a REG to the action of an external electromagnetic (EM) perturbation are also of potential interest in the fields of photonics and plasmonics. Furthermore, it has been recently theorized [1] that the REG might be a candidate for the realization of a natural metamaterial, understood, as proposed originally by Veselago in 1968 [2], as a material that can have simultaneously negative values for its electric permittivity and magnetic permeability.

Although the existence of natural metamaterials has not been reported so far, such systems have already been artificially constructed. A successful design of an artificial metamaterial was reported by Smith *et al* [3] and consisted of a periodic array of metallic split-ring resonators and wires, which exhibited simultaneously negative values of the electric permittivity (ϵ) and magnetic permeability (μ) in a microwave-frequency band of the EM spectrum. Subsequently, metamaterials were realized up to the visible range [4] and all-dielectric metamaterials based on Si/SiO₂ heterostructures have been reported [5].

The possibility that the REG may behave as a natural metamaterial [1] deserves further investigation. To investigate the EM responses of the REG one may adopt the quantum-electrodynamics (QED) formalism for physical systems at finite temperatures [6, 7], within linear response and the random-phase approximation (RPA). In this scheme, it has been shown that, in the limit $T \rightarrow 0$, theoretical results for the electric permittivity agree with

previous non-relativistic calculations performed by Lindhard [8]. Moreover, in the long-wavelength limit both ϵ and μ^{-1} exhibit Drude-like EM responses and may be simultaneously negative [1].

In addition, the validity of the model has been tested in the non-relativistic limit by successfully [9] describing the experimental behavior of the plasmon energy, as a function of both the temperature and wave vector, in low-energy condensed-matter systems such as graphite [10, 11] and tin oxide [12]. The study of the EM response of a REG in the regime of high temperatures and densities is, therefore, in order.

The aim of the present work is to investigate the behavior of the EM response functions of the REG, as functions of the temperature, density, frequency, and wave vector, as well as the EM propagation modes within the REG. This study is organized as follows: In section II we describe the theoretical procedure used for obtaining the EM responses and propagation in the REG. Results are presented in section III and conclusions are in section IV.

II. ELECTROMAGNETIC PROPAGATION

The partition function for QED at finite temperatures in linear response and RPA is given by a quadratic functional integral in Euclidean space over fields obeying $A_\mu(\beta, \vec{x}) = A_\mu(0, \vec{x})$ [1, 6]

$$Z[A] = \oint [dA_\mu] \det[-\partial^2] \exp\left(-\frac{1}{2} \int \tilde{A}_\mu \tilde{\Gamma}_{\mu\nu} \tilde{A}_\nu\right), \quad (1)$$

$$\tilde{\Gamma}_{\mu\nu} = q^2 \delta_{\mu\nu} - \left(1 - \frac{1}{\lambda}\right) q_\mu q_\nu - \tilde{\Pi}_{\mu\nu}. \quad (2)$$

The determinant comes from the Lorentz gauge condition and λ is a gauge parameter. We have used the simplified notation

$$\not\mathcal{F} \equiv \frac{1}{\beta} \sum_{n=-\infty}^{+\infty} \int \frac{d^3q}{(2\pi)^3}, \quad (3)$$

and the polarization tensor of QED [7]

$$\tilde{\Pi}_{\mu\nu} = -\frac{e^2}{\beta} \sum_{n=-\infty}^{+\infty} \int \frac{d^3p}{(2\pi)^3} \text{Sp}[\gamma_\mu G_0(p) \gamma_\nu G_0(p-q)], \quad (4)$$

where G_0 is the free electron propagator at finite density.

One may write $\tilde{\Pi}_{\nu\sigma} = \tilde{\Pi}_{\nu\sigma}^{(v)} + \tilde{\Pi}_{\nu\sigma}^{(m)}$ to separate vacuum and medium contributions. The vacuum contribution is

$$-\frac{\tilde{\Pi}_{\nu\sigma}^{(v)}}{q^2} = \left(\delta_{\nu\sigma} - \frac{q_\nu q_\sigma}{q^2} \right) \mathcal{C}(q^2), \quad (5)$$

whereas the medium contribution is given by

$$-\frac{\tilde{\Pi}_{ij}^{(m)}}{q^2} = \left(\delta_{ij} - \frac{q_i q_j}{|\vec{q}|^2} \right) \mathcal{A} + \delta_{ij} \frac{q_4^2}{|\vec{q}|^2} \mathcal{B}, \quad (6)$$

$$-\frac{\tilde{\Pi}_{44}^{(m)}}{q^2} = \mathcal{B}, \quad -\frac{\tilde{\Pi}_{4i}^{(m)}}{q^2} = -\frac{q_4 q_i}{|\vec{q}|^2} \mathcal{B}, \quad (7)$$

where the three scalar functions $\mathcal{A}(q_4, |\vec{q}|)$, $\mathcal{B}(q_4, |\vec{q}|)$, and $\mathcal{C}(q^2 = q_4^2 + |\vec{q}|^2)$ are determined from the Feynman graph in Eq. (4) [1].

Following [6], we introduce the projector

$$\mathcal{P}_{\mu\nu} = \delta_{\mu\nu} - \frac{q_\mu q_\nu}{q^2}, \quad (8)$$

and the transverse $\mathcal{P}_{\mu\nu}^T$ projector

$$\mathcal{P}_{ij}^T = \delta_{ij} - \hat{q}_i \hat{q}_j, \quad (9)$$

$$\mathcal{P}_{44}^T = \mathcal{P}_{4i}^T = 0, \quad (10)$$

with $\hat{q}_i = q_i/|\vec{q}|$. The longitudinal projector is then $\mathcal{P}_{\mu\nu}^L \equiv \mathcal{P}_{\mu\nu} - \mathcal{P}_{\mu\nu}^T$ so that the polarization tensor is given by

$$\tilde{\Pi}_{\mu\nu} = \tilde{\Pi}_{\mu\nu}^{(v)} + \tilde{\Pi}_{\mu\nu}^{(m)} = \mathcal{F} \mathcal{P}_{\mu\nu}^L + \mathcal{G} \mathcal{P}_{\mu\nu}^T, \quad (11)$$

where

$$\mathcal{F} = -q^2 \left(\mathcal{C} + \mathcal{B} + \frac{q_4^2}{|\vec{q}|^2} \mathcal{B} \right), \quad (12)$$

$$\mathcal{G} = -q^2 \left(\mathcal{C} + \mathcal{A} + \frac{q_4^2}{|\vec{q}|^2} \mathcal{B} \right). \quad (13)$$

The quadratic kernel is then

$$\tilde{\Gamma}_{\mu\nu} = (q^2 - \mathcal{F}) \mathcal{P}_{\mu\nu}^L + (q^2 - \mathcal{G}) \mathcal{P}_{\mu\nu}^T + \frac{1}{\lambda} q_\mu q_\nu, \quad (14)$$

and its inverse, the photon propagator, reads

$$\tilde{\Gamma}_{\mu\nu}^{-1} = \frac{\mathcal{P}_{\mu\nu}^L}{q^2 - \mathcal{F}} + \frac{\mathcal{P}_{\mu\nu}^T}{q^2 - \mathcal{G}} + \frac{\lambda}{q^2} \frac{q_\mu q_\nu}{q^2}. \quad (15)$$

On the other hand, one may also obtain EM responses from the polarization tensor. Indeed, we have recently [1] shown that the (Fourier transformed) constitutive equations of the REG are $D_j = \epsilon_{jk} E_k + \tau_{jk} B_k$, $H_j = \nu_{jk} B_k + \tau_{jk} E_k$, where we have used the notation $\nu \equiv \mu^{-1}$. The linear-response RPA tensors are $\epsilon_{jk} = \epsilon \delta_{jk} + \epsilon' \hat{q}_j \hat{q}_k$, $\nu_{jk} = \nu \delta_{jk} + \nu' \hat{q}_j \hat{q}_k$, and $\tau_{jk} = \tau \epsilon_{jkl} \hat{q}_l$. The eigenvalues of ϵ_{jk} are $\epsilon + \epsilon'$ and ϵ . The eigenvector associated to $\epsilon + \epsilon'$ is along \hat{q}_k , thus longitudinal, whereas the two eigenvectors corresponding to the eigenvalues ϵ are in directions transverse to \hat{q}_k . The same occurs for ν_{jk} , with eigenvalues $\nu + \nu'$ and ν , whereas τ_{jk} is clearly transverse.

The permittivities and inverse permeabilities are determined by the three scalar functions \mathcal{A}^* , \mathcal{B}^* and \mathcal{C}^* , with the asterisk denoting the continuation to Minkowski space, $q_4 \rightarrow i\omega - 0^+$, of the Euclidean scalar functions $\mathcal{A}(q_4, |\vec{q}|)$, $\mathcal{B}(q_4, |\vec{q}|)$ and $\mathcal{C}(q_4^2 + |\vec{q}|^2)$ obtained from the polarization tensor $\tilde{\Pi}_{\mu\nu}$ [1, 13, 14], i.e.,

$$\epsilon = 1 + \mathcal{A}^* + \left(1 - \frac{\tilde{\omega}^2}{\tilde{q}^2} \right) \mathcal{B}^* + \left(2 + \frac{\tilde{\omega}^2}{\tilde{q}^2 - \tilde{\omega}^2} \right) \mathcal{C}^*, \quad (16)$$

$$\nu = 1 + \mathcal{A}^* - 2 \frac{\tilde{\omega}^2}{\tilde{q}^2} \mathcal{B}^* + \left(2 - \frac{\tilde{q}^2}{\tilde{q}^2 - \tilde{\omega}^2} \right) \mathcal{C}^*, \quad (17)$$

$$\epsilon' = -\nu' = - \left[\mathcal{A}^* + \frac{\tilde{q}^2}{\tilde{q}^2 - \tilde{\omega}^2} \mathcal{C}^* \right], \quad (18)$$

and

$$\tau = -\frac{\tilde{\omega}}{\tilde{q}} \left[\frac{\tilde{q}^2}{\tilde{q}^2 - \tilde{\omega}^2} \mathcal{C}^* + \mathcal{B}^* \right]. \quad (19)$$

For the longitudinal responses, one then obtains

$$\epsilon_L = \epsilon + \epsilon' = 1 + \mathcal{C}^* + \left(1 - \frac{\tilde{\omega}^2}{\tilde{q}^2} \right) \mathcal{B}^*, \quad (20)$$

$$\nu_L = \nu + \nu' = 1 + 2\mathcal{C}^* + 2\mathcal{A}^* - 2 \frac{\tilde{\omega}^2}{\tilde{q}^2} \mathcal{B}^*. \quad (21)$$

Our formulae make use of the dimensionless variables $\tilde{q} = |\vec{q}|/q_c$, $\tilde{\omega} = \omega/\omega_c$, $\tilde{\beta} = mc^2\beta$, and $\tilde{\xi} = \xi/(mc^2)$, where $q_c = mc/\hbar$ is the Compton wave vector, $\omega_c = mc^2/\hbar$ is the Compton frequency, $\beta = 1/(k_B T)$, T is the absolute temperature, and ξ is the chemical potential of the electron gas.

We now use Eqs. (12), (13) and write the propagators in Minkowski space by letting $q_4 \rightarrow i\omega - 0^+$, $q^2 = q_4^2 + |\vec{q}|^2 \rightarrow -q^2 = |\vec{q}|^2 - \omega^2$ and $\mathcal{A}, \mathcal{B}, \mathcal{C} \rightarrow \mathcal{A}^*, \mathcal{B}^*, \mathcal{C}^*$. Then, one obtains

$$\frac{1}{q^2 - \mathcal{F}} \rightarrow \frac{1}{-q^2 \epsilon_L}, \quad (22)$$

$$\frac{1}{q^2 - \mathcal{G}} \rightarrow \frac{2}{-q^2 [\nu_L + 1]}. \quad (23)$$

Eq. (22) leads to a pole in the $\mathcal{P}_{\mu\nu}^L$ longitudinal propagator whenever

$$\epsilon_L(\omega, |\vec{q}|) = 0. \quad (24)$$

Note that the pole at $q^2 = 0$ is not realized in this case as it corresponds to a transverse mode, as we shall explicitly show. We remark that (24) corresponds to the usual condensed matter dispersion relation of longitudinal plasmon collective excitations.

The $\mathcal{P}_{\mu\nu}^T$ transverse propagator [cf. Eq. (23)] has poles whenever

$$\begin{aligned} \nu_L(\omega, |\vec{q}|) &= -1, \\ q^2 &= \omega^2 - |\vec{q}|^2 = 0. \end{aligned} \quad (25)$$

Analogously to the longitudinal case, Eq. (25) yields the dispersion relation of transverse plasmon collective excitations whereas Eq. (26) yields a photonic mode that propagates with the speed of light $c (= 1)$ in vacuum.

In order to have more explicit expressions for the plasmon modes, it is useful to write the projectors as

$$\mathcal{P}_{\mu\nu} = n_\mu^{(1)} n_\nu^{(1)} + n_\mu^{(2)} n_\nu^{(2)} + n_\mu^{(3)} n_\nu^{(3)}, \quad (27)$$

$$\mathcal{P}_{\mu\nu}^T = n_\mu^{(1)} n_\nu^{(1)} + n_\mu^{(2)} n_\nu^{(2)}, \quad (28)$$

where $n_\mu^{(i)} = (0, \hat{n}^{(i)})$, $\hat{q} \cdot \hat{n}^{(i)} = 0$, $|\hat{n}^{(i)}| = 1$, for $i = 1, 2$, satisfying $\hat{n}_i^{(1)} \hat{n}_j^{(1)} + \hat{n}_i^{(2)} \hat{n}_j^{(2)} + \hat{q}_i \hat{q}_j = \delta_{ij}$. For $n_\mu^{(3)}$, we find

$$n_\mu^{(3)} = \left(\frac{-|\vec{q}|}{\sqrt{q^2}}, \frac{q_4 \hat{q}}{\sqrt{q^2}} \right), \quad (29)$$

if we demand that it must be normalized and orthogonal to q_μ and $n_\mu^{(i)}$, $i = 1, 2$, thus satisfying $n_\mu^{(1)} n_\nu^{(1)} + n_\mu^{(2)} n_\nu^{(2)} + n_\mu^{(3)} n_\nu^{(3)} + (q_\mu q_\nu / q^2) = \delta_{\mu\nu}$. Then

$$\mathcal{P}_{\mu\nu}^L = n_\mu^{(3)} n_\nu^{(3)}, \quad (30)$$

$$\mathcal{P}_{\mu\nu}^T = n_\mu^{(1)} n_\nu^{(1)} + n_\mu^{(2)} n_\nu^{(2)}. \quad (31)$$

A few observations are in order:

(i) in Minkowski space, we have

$$n_\mu^{(3)} = \left(\frac{i|\vec{q}|}{\sqrt{q^2}}, \frac{\omega \hat{q}}{\sqrt{q^2}} \right), \quad (32)$$

which in the long-wavelength limit becomes $n_\mu^{(3)} = (0, \hat{q})$;

(ii) in that limit, Ref. [1] obtains Drude expressions for $\epsilon_L = 1 - (\omega_e^2 / \omega^2)$ and $\nu_L = 1 - (\omega_m^2 / \omega^2)$. Inserting this into (22) and (23), and using the fact that $\omega_m^2 = 2\omega_e^2$, we find $\omega_e^2 - \omega^2$ as the denominator for both longitudinal and transverse plasmon propagators.

The collective plasmon excitations correspond to charge density and current density oscillations. Indeed,

the collective field $A^L \equiv n_\mu^{(3)} \mathcal{P}_{\mu\nu}^L A_\nu = A_\nu n_\nu^{(3)}$, in Euclidean space, is given by

$$A^L = \frac{-i\vec{q} \cdot (-i\vec{q} A_4 + iq_4 \vec{A})}{\sqrt{q^2} |\vec{q}|} = \frac{-\vec{\nabla} \cdot \vec{E}}{\sqrt{q^2} |\vec{q}|}. \quad (33)$$

Since the field has a longitudinal component, we may define an effective charge density ρ_e as $\vec{\nabla} \cdot \vec{E} \equiv \rho_e(q)$. Similarly, the collective field $A_\mu^T \equiv \mathcal{P}_{\mu\nu}^T A_\nu$ is given by $(0, \vec{A}^T)$, where $\vec{A}^T = A_1 \hat{n}^{(1)} + A_2 \hat{n}^{(2)}$ and $A_i = \vec{A} \cdot \hat{n}^{(i)}$. One then obtains

$$\vec{A}^T = \frac{i\vec{q} \wedge (i\vec{q} \wedge \vec{A})}{|\vec{q}|^2} = \frac{\vec{\nabla} \wedge \vec{B}}{|\vec{q}|^2}. \quad (34)$$

We may then define an effective current density \vec{j}_e through $\vec{\nabla} \wedge \vec{B} = \vec{j}_e$. Then, if we use (12), (13), and (14), and leave aside a gauge term, the plasmon Lagrangean may be written, in Minkowski space, as

$$\rho_e(q) \left(\frac{\epsilon_L}{q^2} \right) \rho_e(q) + j_e^k(q) \left[\frac{(\nu_L + 1)(1 - \frac{\omega^2}{|\vec{q}|^2})}{2q^2} \right] j_e^k(q), \quad (35)$$

where $q = (\omega, \vec{q})$. The above expression physically describes the interaction of charge densities induced by the longitudinal component of the fluctuating electric fields and current densities (loops in the plane perpendicular to \hat{q}) induced by the fluctuating magnetic fields. Apart from that, whenever $\epsilon_L \neq 0$ and $\nu_L \neq -1$, we just have the propagation of an electromagnetic wave with a propagator given by (23).

An alternative and somewhat complementary analysis may be obtained from Maxwell's equations combined with the constitutive relations written out previously. Maxwell's equations are (we have now restored the speed of light c)

$$q_i D_i = 0, \quad (36a)$$

$$q_i B_i = 0, \quad (36b)$$

$$\epsilon_{ijk} q_j E_k = \frac{\omega}{c} B_i, \quad (36c)$$

and

$$\epsilon_{ijk} q_j H_k = -\frac{\omega}{c} D_i. \quad (36d)$$

The constitutive equations were defined in the paragraph after Eq. (15). From Eq. (36a) and the constitutive relations, we derive

$$(\vec{q} \cdot \vec{E}) \epsilon_L = 0. \quad (37)$$

If $\epsilon_L \neq 0$, then we must have $\vec{q} \cdot \vec{E} = 0$, so that Eq. (36d) and the constitutive relations give

$$\left[\tau |\vec{q}| + \epsilon \frac{\omega}{c} \right] \vec{E} + \left[\nu |\vec{q}| - \tau \frac{\omega}{c} \right] (\hat{q} \wedge \vec{B}) = 0, \quad (38)$$

which combined with Eq. (36c) yields a generalized wave equation [15] for \vec{E} (and an analogous one for \vec{B})

$$\left[|\vec{q}|^2 - \mu\epsilon \frac{\omega^2}{c^2} - 2\mu\tau |\vec{q}| \frac{\omega}{c} \right] \vec{E} = 0. \quad (39)$$

However, using Eqs. (16) to (19), (20) and (21), Eq. (38) becomes

$$(\nu_L + 1)[\vec{q} \wedge \vec{B} + \frac{\omega}{c} \vec{E}] = 0, \quad (40)$$

whereas Eq. (39) yields

$$(\nu_L + 1)q^2 = (\nu_L + 1) \left[\frac{\omega^2}{c^2} - |\vec{q}|^2 \right] = 0. \quad (41)$$

We see that Maxwell's equation (36a) will be satisfied if $\epsilon_L = 0$. This coincides with the longitudinal plasmon condition. If $\epsilon_L \neq 0$, then \vec{E} is transverse and eq. (41) will be satisfied if either $\nu_L = -1$ (transverse plasmons) or $q^2 = 0$ (photons). The fact that the wave equation factors out into two terms is a consequence of the specific form of the EM responses for the REG.

Before proceeding, we note that $\mathcal{A}^*, \mathcal{B}^*, \mathcal{C}^*$ are given explicitly by

$$\mathcal{A}^* = \frac{A_\alpha}{\tilde{q}^2 - \tilde{\omega}^2} \mathcal{I} + \left[1 - \frac{3}{2} \frac{\tilde{q}^2 - \tilde{\omega}^2}{\tilde{q}^2} \right] \mathcal{B}^*, \quad (42)$$

$$\mathcal{B}^* = \frac{B_\alpha}{\tilde{q}^2 - \tilde{\omega}^2} \mathcal{J}, \quad (43)$$

and

$$\mathcal{C}^* = -C_\alpha \left\{ \frac{1}{3} + (3 + \gamma^2) [\gamma \operatorname{arccot}(\gamma) - 1] \right\}, \quad (44)$$

where

$$\gamma = \sqrt{\frac{4}{\tilde{\omega}^2 - \tilde{q}^2} - 1}, \quad (45)$$

$A_\alpha = B_\alpha = 4\alpha/\pi$, $C_\alpha = A_\alpha/12$, α is the fine-structure constant, and the functions \mathcal{I} and \mathcal{J} are the one-dimensional integrals

$$\begin{aligned} \mathcal{I} &= \int_0^\infty dy \frac{y^2}{\sqrt{y^2+1}} \mathcal{F}_0(y, \tilde{\beta}, \tilde{\xi}) \\ &\times \left[1 + \frac{2 - \tilde{q}^2 + \tilde{\omega}^2}{8y\tilde{q}} \mathcal{F}_1(y, \tilde{q}, \tilde{\omega}) \right] \end{aligned} \quad (46)$$

and

$$\begin{aligned} \mathcal{J} &= \int_0^\infty dy \frac{y^2}{\sqrt{y^2+1}} \mathcal{F}_0(y, \tilde{\beta}, \tilde{\xi}) \\ &\times \left[1 + \frac{4(y^2+1) - \tilde{q}^2 + \tilde{\omega}^2}{8y\tilde{q}} \mathcal{F}_1(y, \tilde{q}, \tilde{\omega}) \right. \\ &\left. - \frac{\tilde{\omega}\sqrt{y^2+1}}{2y\tilde{q}} \mathcal{F}_2(y, \tilde{q}, \tilde{\omega}) \right], \end{aligned} \quad (47)$$

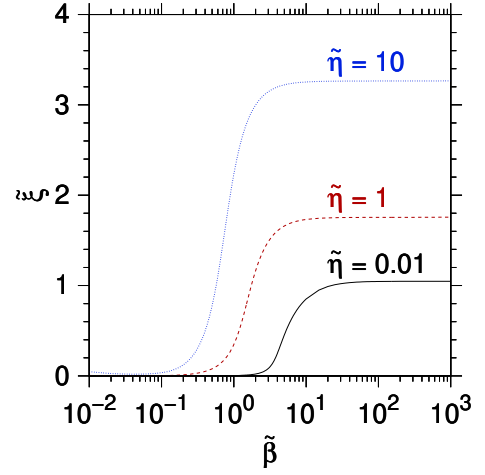


FIG. 1: (Color online) Chemical potential as a function of the gas temperature. Solid, dashed, and dotted lines correspond to $\tilde{\eta} = 0.01$, $\tilde{\eta} = 1$, and $\tilde{\eta} = 10$, respectively.

respectively. The functions $\mathcal{F}_0, \mathcal{F}_1$ and \mathcal{F}_2 are defined as

$$\mathcal{F}_0(y, \tilde{\beta}, \tilde{\xi}) = \frac{1}{e^{\tilde{\beta}(\sqrt{y^2+1}-\tilde{\xi})} + 1} - \frac{1}{e^{\tilde{\beta}(\sqrt{y^2+1}+\tilde{\xi})} + 1}, \quad (48)$$

$$\mathcal{F}_1(y, \tilde{q}, \tilde{\omega}) = \ln \left[\frac{(\tilde{q}^2 - \tilde{\omega}^2 + 2y\tilde{q})^2 - 4(y^2 + 1)\tilde{\omega}^2}{(\tilde{q}^2 - \tilde{\omega}^2 - 2y\tilde{q})^2 - 4(y^2 + 1)\tilde{\omega}^2} \right], \quad (49)$$

and

$$\mathcal{F}_2(y, \tilde{q}, \tilde{\omega}) = \ln \left[\frac{\tilde{\omega}^4 - 4(\tilde{\omega}\sqrt{y^2+1} + y\tilde{q})^2}{\tilde{\omega}^4 - 4(\tilde{\omega}\sqrt{y^2+1} - y\tilde{q})^2} \right]. \quad (50)$$

respectively.

III. RESULTS AND DISCUSSION

A. The chemical potential

To compute the electromagnetic responses of the REG through Eqs.(16)-(19), one needs to obtain the ξ chemical potential which depends on the temperature and carrier density. The carrier density is $\eta = \Delta N/V$, where $\Delta N = N^- - N^+$ is the difference between the N^- number of particles and the N^+ number of antiparticles in the system. Then, one needs to solve the transcendental equation [1]

$$\Delta N = N^- - N^+ = \sum_{\vec{p}} g f(p, \beta, \xi), \quad (51)$$

where

$$f(p, \beta, \xi) = \frac{1}{e^{\beta(\Omega_p - \xi)} + 1} - \frac{1}{e^{\beta(\Omega_p + \xi)} + 1} \quad (52)$$

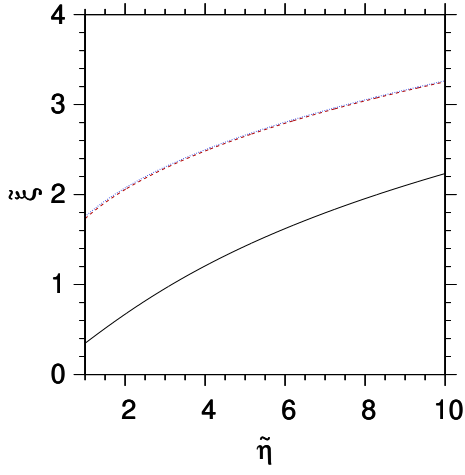


FIG. 2: (Color online) Chemical potential as a function of the gas density. Solid, dashed, and dotted lines correspond to $\tilde{\beta} = 1$, $\tilde{\beta} = 10$, and $\tilde{\beta} = 100$, respectively.

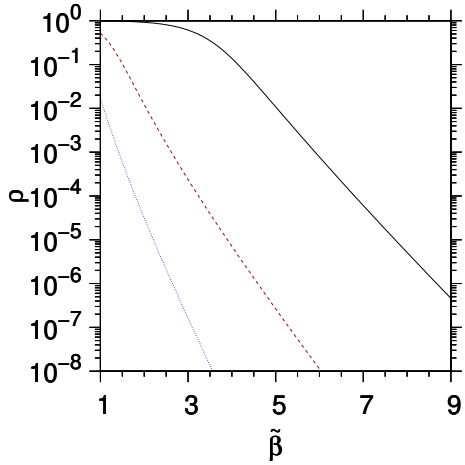


FIG. 3: (Color online) The ratio $\rho = N^+/N^-$ [cf. Eq. (54)] as a function of $\tilde{\beta}$. Solid, dashed, and dotted lines correspond to $\tilde{\eta} = 0.01$, $\tilde{\eta} = 1$, and $\tilde{\eta} = 10$, respectively.

is the distribution function accounting for the presence of both particles and antiparticles, $\Omega_p = \sqrt{p^2 c^2 + m^2 c^4}$ is the relativistic energy of a carrier with momentum p , and $g = 2$ is the degeneracy factor of the electron gas. Eq. (51) reduces to

$$\tilde{\eta} = \frac{\eta}{\eta_0} = \int_0^{+\infty} dy y^2 \mathcal{F}_0(y, \tilde{\beta}, \tilde{\xi}) \quad (53)$$

where $\eta_0 = g q_c^3 / (2\pi^2) \approx 1.76 \times 10^{30} \text{ cm}^{-3}$ only depends on universal constants and may, therefore, be used as a natural unit to measure the η effective carrier density of the REG. It should be noted [Eq. (48)] that $\mathcal{F}_0(y, \tilde{\beta}, -\tilde{\xi}) = -\mathcal{F}_0(y, \tilde{\beta}, \tilde{\xi})$, i.e., $\mathcal{F}_0 = \mathcal{F}_0(y, \tilde{\beta}, \tilde{\xi})$ is an odd function of the chemical potential. Eq. (53) implicitly defines the function $\tilde{\xi} = \tilde{\xi}(\tilde{\beta}, \tilde{\eta})$. One sees that

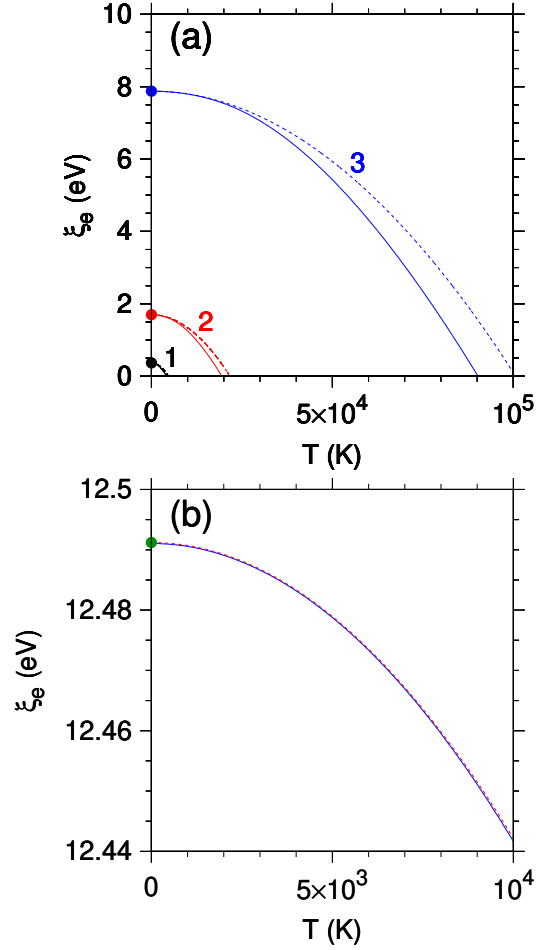


FIG. 4: (Color online) Chemical potential, measured with respect to the mc^2 rest energy [cf. Eq. (55)], as a function of the gas temperature for different values of the η gas density. Solid and dashed lines corresponds to numerical results obtained from Eqs. (53) and (56), respectively. The set of curves 1, 2, and 3 in panel (a) correspond to $\eta = 10^{21} \text{ cm}^{-3}$, $\eta = 10^{22} \text{ cm}^{-3}$, and $\eta = 10^{23} \text{ cm}^{-3}$, respectively. In panel (b), calculations were performed for η corresponding to the electron density in silicon. The full dot in the left vertical axis corresponds to the Fermi energy obtained from Eq. (57).

$\tilde{\xi} = 0$ leads to $\eta/\eta_0 = 0$, a case with corresponds to vacuum.

The chemical potential as a function of $\tilde{\beta}$ is displayed in Fig. 1. Calculations were performed for three different values of the density expressed in units of η_0 . The numerical results suggest a weak temperature dependence of the chemical potential, if compared with $mc^2 \approx 0.511 \text{ MeV}$, in the low-temperature limit ($\tilde{\beta} \rightarrow \infty$). Actually, the chemical potential exhibits variations of a few eV in the low-temperature limit, a fact which agrees with the non-relativistic theory of the electron gas (see below).

The chemical potential is displayed in Fig. 2 as a function of the density expressed in units of η_0 . Numerical results were obtained for three different values of the gas temperature. The chemical potential is a growing mono-

tonic function of $\tilde{\eta}$. One may note that the chemical potentials for $\tilde{\beta} = 10$ and $\tilde{\beta} = 100$ essentially coincide in the scale of the figure [cf. dashed and dotted lines in Fig. 2].

The ratio

$$\rho = \frac{N^+}{N^-} = \frac{\int_0^{+\infty} dy \frac{y^2}{e^{\tilde{\beta}(\sqrt{y^2+1}+\xi)}+1}}{\int_0^{+\infty} dy \frac{y^2}{e^{\tilde{\beta}(\sqrt{y^2+1}-\xi)}+1}}. \quad (54)$$

as a function of $\tilde{\beta}$ is displayed in Fig. 3 for various values of the density. For a given temperature, it is apparent that the number of particles exceeds the number of antiparticles in all cases and the ratio $\rho = N^+/N^-$ decreases as the density of particles in the electron gas is increased, as expected. One may also note that $\rho \rightarrow 0$ as $\tilde{\beta} \rightarrow \infty$, since in the low-temperature limit one has $N^+ \ll N^-$. In other words, in the limit $\tilde{\beta} \rightarrow \infty$, the term corresponding to the occupation factor of antiparticles in the Fermi-Dirac distribution function [cf. the second term in the RHS of Eq. (52)] may essentially be neglected ($N^+ \ll N^-$) and the non-relativistic limit of the Fermi-Dirac distribution function is eventually recovered.

We have also explored the behavior of the chemical potential for density and temperature values appropriate for solid-state materials. In this respect, we have defined

$$\xi_e(T) = \xi(T) - mc^2 \quad (55)$$

as the non-relativistic chemical potential. According to the non-relativistic theory of the free-electron gas, it is well known that

$$\xi_e(T) \approx E_F \left[1 - \frac{\pi^2}{12} \left(\frac{T}{T_F} \right)^2 \right], \quad (56)$$

where

$$E_F = \left(\frac{6\pi^2}{g} \eta \right)^{\frac{2}{3}} \frac{\hbar^2}{2m}, \quad (57)$$

is the Fermi energy and $T_F = E_F/k_B$ is the Fermi temperature. The ξ_e chemical potential is depicted in Fig. 4 as a function of the gas temperature. Calculations in Fig. 4(a) were performed for three different values of η varying within the range exhibited by most of the solid-state materials. In Fig. 4(b) we have assumed $\eta \approx 2.0 \times 10^{23} \text{ cm}^{-3}$ corresponding to the electron density in silicon. The solid line corresponds to the result computed by combining Eqs. (53) and (55), whereas the dashed line was obtained from Eq. (56). The Fermi energy computed from the non-relativistic electron-gas model [cf. full dot in the vertical axis of Fig. 4(b) and Eq. (57)] essentially coincides with the numerical result obtained from Eqs. (53) and (55) in the limit $T \rightarrow 0$. Low-temperature results obtained from the non-relativistic model agree with those derived from the relativistic theory, as expected.

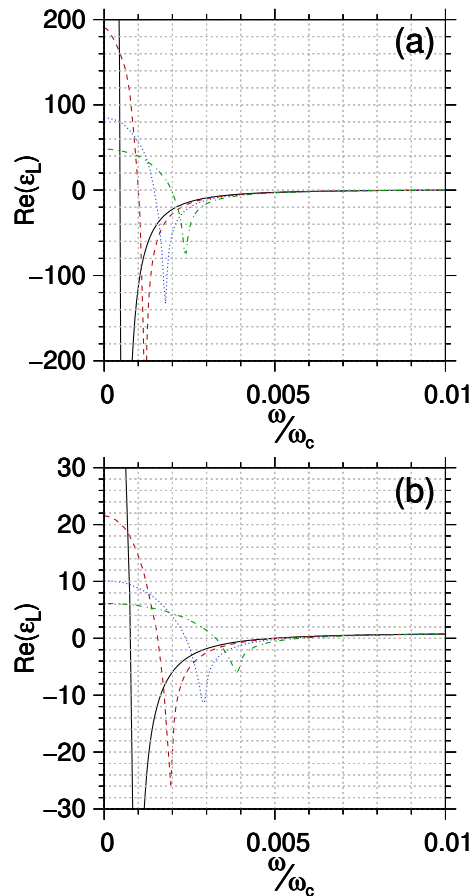


FIG. 5: (Color online) Real part of ϵ_L as a function of the ω frequency in units of the ω_c Compton frequency, for various values of the wave vector $|\tilde{q}|$ expressed in units of the q_c Compton wave vector, and for $\tilde{\eta} = 0.01$. Results of panels (a) and (b) were obtained for $\tilde{\beta} = 1000$ and $\tilde{\beta} = 1$, respectively. Solid, dashed, dotted, and dot-dashed lines in panel (a) [(b)] correspond to $\tilde{q} = 0.002$, $\tilde{q} = 0.004$, $\tilde{q} = 0.006$, and $\tilde{q} = 0.008$, respectively ($\tilde{q} = 0.001$, $\tilde{q} = 0.002$, $\tilde{q} = 0.003$, and $\tilde{q} = 0.004$, respectively).

B. Longitudinal plasmon modes of the REG

Now we focus our attention on the ϵ_{ij} electric permittivity tensor. According to Eq. (20) one has

$$\epsilon_L = \epsilon + \epsilon' = 1 + \mathcal{C}^* + \left(1 - \frac{\tilde{\omega}^2}{\tilde{q}^2} \right) \mathcal{B}^*, \quad (58)$$

The real part of ϵ_L is depicted in Fig. 5 as a function of ω in units of ω_c . Results were computed for $\tilde{\eta} = 0.01$ and different values of $|\tilde{q}|$ expressed in units of q_c . In Figs. 5(a) and 5(b) we have set $\tilde{\beta} = 1000$ and $\tilde{\beta} = 1$, respectively. The real part of the longitudinal electric permittivity exhibits two zeros for a given value of \tilde{q} at a given temperature. The lower zero lies within a region where $\text{Im}[\epsilon_L] \neq 0$. Therefore, in spite of the fact that $\text{Re}[\epsilon_L] = 0$ in this case, such a zero cannot be considered

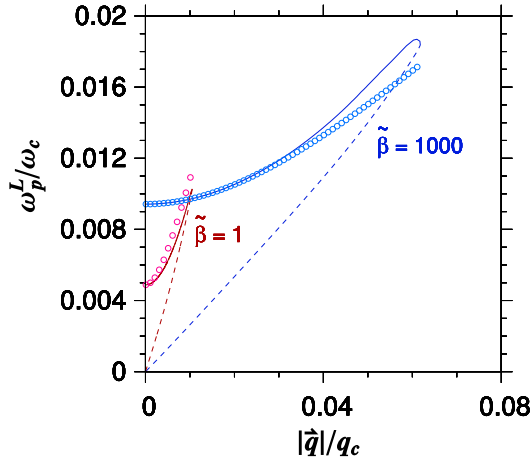


FIG. 6: (Color online) Upper (ω_p^L longitudinal plasmon frequency) and lower frequency zeros of ϵ_L as functions of the $|\tilde{q}|$ wave vector. Calculations were performed for $\tilde{\beta} = 1$ and $\tilde{\beta} = 1000$, by taking $\tilde{\eta} = 0.01$. Open circles correspond to the analytical results obtained from Eq. (65). Both ω and $|\tilde{q}|$ are expressed in units of ω_c and q_c , respectively.

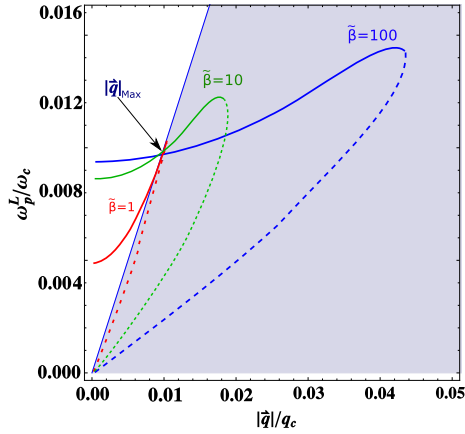


FIG. 7: (Color online) Upper (ω_p^L plasmon frequency) and lower frequency zeros of ϵ_L (solid and dashed lines, respectively) as functions of the $|\tilde{q}|$ wave vector. Calculations were performed for $\tilde{\beta} \rightarrow \infty$ ($T = 0$), $\tilde{\beta} = 100$, $\tilde{\beta} = 10$ and $\tilde{\beta} = 1$ by taking $\tilde{\eta} = 0.01$. The shaded area corresponds to the region where electron-hole excitations occur. Note the maximum value of the wave vector (\tilde{q}_{max}) beyond which the longitudinal plasmon decays into electron-hole pairs. Both the frequency and wave vector are given in units of ω_c and q_c , respectively.

as a plasmon frequency. In the vicinity of the upper zero, on the other hand, one may have $\text{Im}[\epsilon_L] = 0$ (see discussion below), so that it corresponds to the ω_p^L longitudinal plasmon frequency. We then show in Fig. 6 the upper (solid lines) and lower (dashed lines) frequency zeros of the real part of ϵ_L as functions of \tilde{q} . Numerical calculations were performed for $\tilde{\eta} = 0.01$ and two different values of $\tilde{\beta}$.

For sufficiently small values of the \tilde{q} wave vector, the

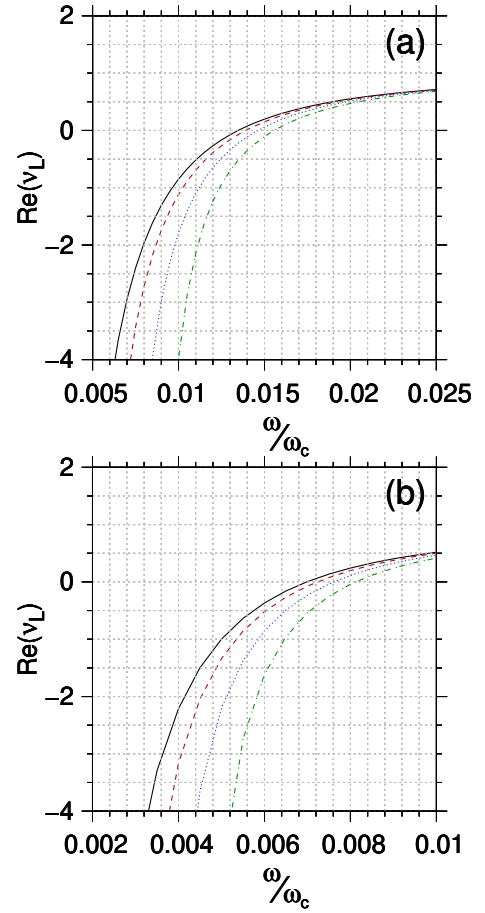


FIG. 8: (Color online) Real parts of ν_L as a function of the ω frequency in units of the ω_c Compton frequency, for various values of the wave vector $|\tilde{q}|$ given in units of the q_c Compton wave vector. Calculations were performed for $\tilde{\eta} = 0.01$. Results of panels (a) [(b)] were obtained for $\tilde{\beta} = 1000$ ($\tilde{\beta} = 1$). Solid, dashed, dotted, and dot-dashed lines in panels (a) [(b)] correspond to $\tilde{q} = 0.002$, $\tilde{q} = 0.004$, $\tilde{q} = 0.006$, and $\tilde{q} = 0.008$, respectively ($\tilde{q} = 0.001$, $\tilde{q} = 0.002$, $\tilde{q} = 0.003$, and $\tilde{q} = 0.004$, respectively).

longitudinal-plasmon dispersion relation may be approximately described by the expression

$$(\tilde{\omega}_p^L)^2 = (\tilde{\omega}_{0p}^L)^2 + \frac{v_T^2}{c^2} \tilde{q}^2, \quad (59)$$

where the frequencies and wave vector are given in units of ω_c and q_c , respectively. In the above expression $\tilde{\omega}_{0p}^L$ is the temperature-dependent longitudinal plasmon frequency in the long-wavelength limit and v_T plays the role of the carrier thermal speed, except for a numeric factor. The low-temperature non-relativistic case $v_T^2 = 3/(m\beta)$ leads to the well-known Bohm-Gross dispersion relation [16]. To estimate the carrier thermal speed corresponding to the REG, we have computed the average of p^2 from

the expression

$$\langle p^2 \rangle = \frac{\sum_{\vec{p}} g p^2 f(p, \beta, \xi)}{\sum_{\vec{p}} g f(p, \beta, \xi)}, \quad (60)$$

which reduces to

$$\langle p^2 \rangle = m^2 c^2 \mathcal{K}(\tilde{\beta}, \tilde{\xi}), \quad (61)$$

where

$$\mathcal{K}(\tilde{\beta}, \tilde{\xi}) = \frac{1}{\tilde{\eta}} \int_0^{+\infty} dy y^4 \mathcal{F}_0(y, \tilde{\beta}, \tilde{\xi}). \quad (62)$$

The v_T carrier thermal speed is given by

$$\langle p^2 \rangle = \frac{m^2}{1 - \frac{v_T^2}{c^2}} v_T^2, \quad (63)$$

which results in

$$v_T^2 = c^2 \frac{\mathcal{K}(\tilde{\beta}, \tilde{\xi})}{1 + \mathcal{K}(\tilde{\beta}, \tilde{\xi})}. \quad (64)$$

Then Eq. (59) becomes

$$(\tilde{\omega}_p^L)^2 = (\tilde{\omega}_{0p}^L)^2 + \frac{\mathcal{K}(\tilde{\beta}, \tilde{\xi})}{1 + \mathcal{K}(\tilde{\beta}, \tilde{\xi})} \tilde{q}^2. \quad (65)$$

The above equation is a generalization of the Bohm-Gross dispersion relation to the case of a REG at finite temperatures and is valid in the limit $\tilde{q} \ll \tilde{q}_{max}$, i.e, far from the region where electron-hole excitations occur. Theoretical results obtained from Eq. (65) are displayed in Fig. 6 as open circles, for both $\tilde{\beta} = 1$ and $\tilde{\beta} = 1000$, and for $\tilde{\eta} = 0.01$. In the long-wavelength regime, the agreement with the curve from Eq. (24) is quite good.

We display in Fig. 7 the upper (solid lines) and lower (dashed lines) frequency zeros of the real part of ϵ_L as functions of $\tilde{q} = |\tilde{q}|/q_c$. Numerical results were computed for $\tilde{\eta} = 0.01$ and different values of $\tilde{\beta}$. Fig. 7 clearly indicates that there is a maximum value of the wave vector (\tilde{q}_{max}) beyond which the longitudinal plasmon decays into electron-hole pairs.

C. Transverse plasmon modes of the REG

The condition $\nu_L = -1$ [cf. (25)] leads to the ω_p^T frequency of the REG transverse plasmon modes. We display in Fig. 8 the real part of ν_L as a function of the ω frequency in units of ω_c , obtained for $\tilde{\eta} = 0.01$ and different values of the wave vector $|\tilde{q}|$ in units of q_c . Results depicted in Figs. 8(a) and 8(b) where computed for $\tilde{\beta} = 1000$ and $\tilde{\beta} = 1$, respectively. We would like to stress that numerical results (not shown here) indicate that $\text{Im}[\nu_L] = 0$ within the respective frequency

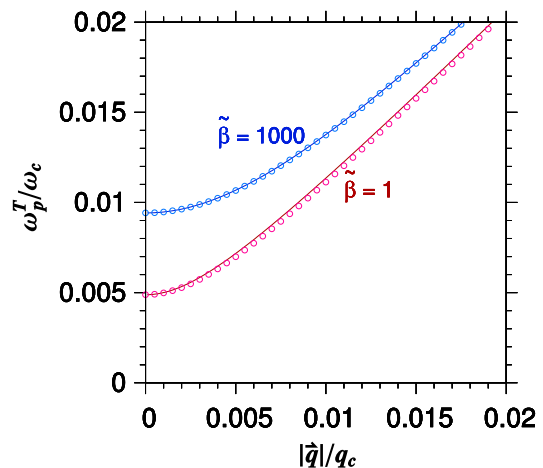


FIG. 9: (Color online) Transverse plasmon frequency (zero of $\nu_L + 1 = 0$) as a function of the $|\tilde{q}|$ wave vector. The ω_p^T transversal plasmon frequency and the $|\tilde{q}|$ wave vector are given in units of the ω_c Compton frequency and q_c Compton wave vector, respectively. Solid lines correspond to theoretical results obtained from $\nu_L + 1 = 0$. Calculations were performed for $\tilde{\beta} = 1$ and $\tilde{\beta} = 1000$, by taking $\tilde{\eta} = 0.01$. Open circles correspond to the analytical results obtained from Eq. (66).

ranges considered in both Fig. 8(a) and 8(b). Therefore, in the present cases, the transversal plasmon frequencies can be obtained by solving the transcendental equation $\text{Re}[\nu_L] = -1$.

The ω_p^T transverse plasmon frequency is displayed in Fig. 9 as a function of the $\tilde{q} = |\tilde{q}|/q_c$ wave vector for different values of the gas temperature. Calculations were performed for $\tilde{\eta} = 0.01$. Solid lines correspond to the numerical results obtained from $\nu_L = -1$ [cf. Eq.(25)]. Such results indicate the existence of one single positive zero of $\nu_L + 1$ for a given value of \tilde{q} at a given gas temperature. Therefore, the dispersion exhibits only a single branch. We also note that, at a given temperature, the wave vector dependence of the resonance frequency may be approximated by

$$(\tilde{\omega}_p^T)^2(q) = (\tilde{\omega}_{0p}^T)^2 + \tilde{q}^2, \quad (66)$$

which fits quite well the numerical results obtained from Eq. (25). In the above equation $\tilde{\omega}_{0p}^T$ is the temperature-dependent transverse plasmon frequency numerically obtained from Eq. (25) in the limit $\tilde{q} \rightarrow 0$. Results obtained from Eq. (66) are displayed in Fig. 9 as open circles.

D. Decays and responses of the REG

We display in Fig. 10 the dispersion curves for the transverse and longitudinal plasmon modes at $T = 0$ [cf. Eqs. (24) and (25)]. The shaded area corresponds to the region where the excitation of electron-hole pairs occurs. The dashed line is discarded as a solution for the longitudinal plasmon dispersion as it lies entirely in

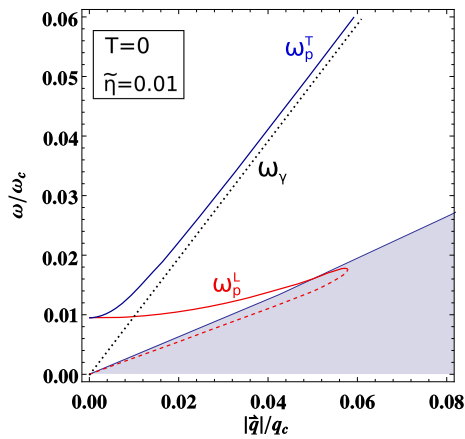


FIG. 10: (Color online) The dispersion curves for transverse and longitudinal plasmon modes at $T = 0$ and $\tilde{\eta} = 0.01$ [cf. Eqs. (24) and (25)]. In the shaded area, $\text{Im}[\epsilon_L] \neq 0$, indicating decay of the longitudinal mode. The dashed line is discarded as a solution for the longitudinal dispersion as it lies entirely in the region of nonzero imaginary part of ϵ_L . We have also shown the dispersion (dotted line) for the photon mode $\tilde{\omega}_\gamma = \tilde{q}$ [see Eq. (26)].

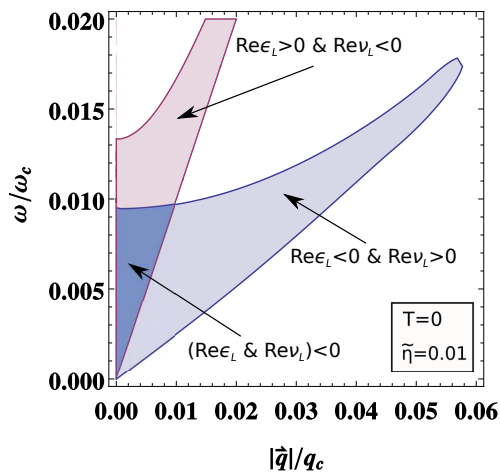


FIG. 11: (Color online) Regions of the $(\tilde{q}, \tilde{\omega})$ plane according to the signs of the real parts of ϵ_L and ν_L . Outside the shaded regions the real parts of ϵ_L and ν_L are positive. Results were obtained for $T = 0$ and $\tilde{\eta} = 0.01$.

the region of nonzero imaginary part of ϵ_L . We have also shown the dispersion for the photon mode $\tilde{\omega}_\gamma = \tilde{q}$ [cf. (26)]. Although not shown in the figure, the straight

dotted line for the photon dispersion will eventually reach the upper region where the excitation of electron-positron pairs will take place [1].

Finally, we display in Fig. 11 the different relevant regions of the $(\tilde{q}, \tilde{\omega})$ plane where the real parts of ϵ_L and ν_L have different signs [17]. We would like to stress there is a region where both ϵ_L and ν_L are simultaneously negative, indicating that the REG exhibits a behavior has not been experimentally observed in natural materials. This fact was previously remarked by one of the authors [1], as mentioned. It is important to note that, in contrast to the non-relativistic case where the refractive index is defined as $n = \sqrt{\epsilon} \sqrt{\mu}$, simultaneous negative values of ϵ_L and ν_L observed in the present relativistic case do not necessarily imply negative refraction. A detailed study of the refractive index of the REG will be the subject of a further work.

IV. CONCLUSIONS

Summing up, we have presented a theoretical study of the EM propagation and responses of a REG for various temperatures and carrier densities. Using linear response and RPA, we have identified the propagation modes and their dispersion relations from the QED propagators as well as from Maxwell's equations with the added input of the constitutive relations obtained from the QED responses. We found a longitudinal plasmon mode, two transverse plasmon modes, and a photonic mode which propagates with the speed of light in vacuum, i.e., for which the medium is transparent thanks to the specific form of its relativistic electromagnetic responses. In deriving dispersion relations, we were able to identify stable solutions and regions of instability where the plasmon modes decay. Finally, we have also identified the regions in the $(|\tilde{q}|, \omega)$ plane where the longitudinal permittivity ϵ_L and longitudinal inverse permeability ν_L are both simultaneously negative.

Acknowledgments

The authors would like to thank the Scientific Colombian Agency CODI - University of Antioquia, and Brazilian Agencies CNPq, CAPES, FAPESP, and FAEPEX/UNICAMP for partial financial support.

-
- [1] C. A. A. de Carvalho, Phys. Rev. D **93**, 105005 (2016).
 - [2] V. G. Veselago, Sov. Phys. Usp. **10**, 509 (1968).
 - [3] D. R. Smith, Willie J. Padilla, D. C. Vier, S. C. Nemat-Nasser, and S. Schultz, Phys. Rev. Lett. **84**, 4184 (2000).
 - [4] N. I. Zheludev, Science **348**, 973 (2015) and references therein.
 - [5] P. Moitra, Y. Yang, Z. Anderson, I. I. Kravchenko, D. P.

- Briggs, and J. Valentine, Nat. Photonics **7**, 791 (2013).
- [6] J. I. Kapusta and C. Gale, *Finite-Temperature Field Theory* (Cambridge University Press, Cambridge, England, 2006).
- [7] I. A. Akhiezer and S. V. Peletminskii, Sov. Phys. JETP **11**, 1316 (1969); E. S. Fradkin, *Proceedings of the P. N. Lebedev Physics Institute*, vol. 29, Consultants Bureau

- (1967).
- [8] J. Lindhard, K. Dan. Vidensk. Selsk., Mat. Fys. Medd. **28**, 8 (1954).
 - [9] E. Reyes-Gómez, L. E. Oliveira, and C. A. A. de Carvalho, Europhys. Lett. **114**, 17009 (2016).
 - [10] E. T. Jensen, R. E. Palmer, W. Allison, and J. F. Annett, Phys. Rev. Lett. **66**, 492 (1991).
 - [11] M. Portail, M. Carrere, and J. M. Layet, Surf. Sci. **433-435**, 863 (1999).
 - [12] X. Zou, J. Luo, D. Lee, C. Cheng, D. Springer, S. K. Nair, S. A. Cheong, H. J. Fan, and E. E. M. Chia, J. Phys. D: Appl. Phys. **45**, 465101 (2012).
 - [13] We note that Eqs. (16)-(19) correct some sign misprints in the corresponding Eqs. in Ref. [9].
 - [14] C. Itzykson and J. B. Zuber, *Quantum Field Theory* (McGraw-Hill, New-York, 1980).
 - [15] Eqs. (38) and (39) correct sign misprints in Eqs. (47)-(49) of Ref. [1]. The correct form of the latter may be obtained by letting $\omega \rightarrow -\omega$.
 - [16] D. Bohm and E. P. Gross, Phys. Rev. **75**, 1851 (1949); *ibid.*, Phys. Rev. **75**, 1864 (1949).
 - [17] C. A. A. de Carvalho and D. M. Reis (unpublished).